Geophysical Research Letters

RESEARCH LETTER
10.1029/2018GL078998

Key Points:
- A contour-following analysis is applied to water vapor to portray the hydrological cycle and its future changes over the Asian monsoon regions
- The resultant water vapor wave activity sink serves as a metric for hydrological extremes
- The hydrological cycling rate increases/decreases in the Indian/East Asian monsoons, although hydrological cycle increases in both regions

Supporting Information:
- Supporting Information S1

Correspondence to:
J. Lu,
jian.lu@pnnl.gov

Citation:
Xue, D., Lu, J., Leung, L. R., & Zhang, Y. (2018). Response of the hydrological cycle in Asian monsoon systems to global warming through the lens of water vapor wave activity analysis. *Geophysical Research Letters*, *45*, 11,904–11,912. https://doi.org/10.1029/2018GL078998

Received 30 MAY 2018
Accepted 9 OCT 2018
Accepted article online 15 OCT 2018
Published online 4 NOV 2018

©2018. American Geophysical Union. All Rights Reserved.

Response of the Hydrological Cycle in Asian Monsoon Systems to Global Warming Through the Lens of Water Vapor Wave Activity Analysis

Daokai Xue[1], Jian Lu[2], L. Ruby Leung[2], and Yaocun Zhang[1]

[1]School of Atmospheric Sciences, Nanjing University, Nanjing, China, [2]Atmospheric Sciences and Global Change Division, Pacific Northwest National Laboratory, Richland, WA, USA

Abstract The column integrated water vapor (CWV)-based local wave activity (LWA) is adapted to examine the response of the hydrological cycle and extremes of the Asian summer monsoon in CMIP5 simulations under the RCP8.5 forcing scenario. A tight linear relationship between CWV LWA (A^+) and its sink ($\widetilde{P-E}^+$), which measures the intensity of the local hydrological cycle and extremes, affords a simple scaling framework for the hydrological cycle intensity in terms of the contributions from (i) ratio of moisture participating in the hydrological cycle, (ii) stirring length scale, (iii) background moisture gradient, and (iv) hydrological cycling rate. Future CWV LWA over the broad Asian monsoon region shows a large increase (~35%), attributable largely to the increase of the background moisture. The scaling analysis reveals a distinct mix of the contributing factors for the increase in $\left(\widetilde{P-E}^+\right)$ between East Asian and Indian monsoon regions, despite both experiencing sizable increase of $\left(\widetilde{P-E}^+\right)$.

Plain Language Summary Budget following the material isoline can bring unique physical insight compared to the conventional budget at fixed point. This approach is applied to the output of the hydrological variables from CMIP5 simulations for both present and future climates to give a "hydrological cycle" perspective to the summer monsoonal rainfall over the Asian monsoon regions. It is found that, under the RCP8.5 warming scenario, the hydrological cycle measured by quantity $\left(\widetilde{P-E}^+\right)$ is intensified over the broad Asian monsoon regions, implicative of a robust increase of the hydrological extremes there, while the hydrological cycling rate, measured by the inverse of the residence time of the integrated column moisture, shows distinct features between the Indian and Southeast Asian monsoon regions.

1. Introduction

It has been well established that anthropogenic climate warming can enhance the hydrological cycle measured by the global mean precipitation (P), or equivalently the global mean evaporation (E; Allen & Ingram, 2002; Held & Soden, 2006; Meehl et al., 2007). If one defines the hydrological cycling rate (HCR) as ratio of the global mean precipitation to the globally integrated water vapor $[P]/[Q]$, the HCR tends to weaken in response to increasing greenhouse gas concentrations, because the rate of the increase of P is not commensurate with that of Q, as the latter follows roughly the Clausius-Clapeyron relation at a rate of ~7% per Kelvin warming (Pall et al., 2007; Santer et al., 2007; Trenberth et al., 2003). This mismatch has been well understood as the result of the radiative response to climate warming: The radiative properties of the atmospheric compositions restrain the radiative cooling from changing as much as the rate of the water vapor (e.g., Stephens & Hu, 2010; Pendergrass & Hartmann, 2014 JC). However, these globally integrated properties, especially the important notion of the weakening of the HCR, cannot be automatically carried over to regional hydrological cycle, which is more important for understanding regional climate impacts.

Lately, Lu et al. (2017, 2018) developed a contour following analysis of column integrated water vapor (CWV)-based local wave activity (LWA) budget to extend the concept of hydrological cycle to regional precipitation and hydrological extremes, with a particular application to features like atmospheric rivers (e.g., Neiman et al., 2011; Ralph et al., 2006; Zhu & Newell, 1998). The essence of the water vapor wave activity is that it allows areal or line integration over regions or intervals districted by contours of CWV (M), which, together with its corresponding equivalent latitude (ϕ_e), serve as the boundary of moisture "reservoirs" for

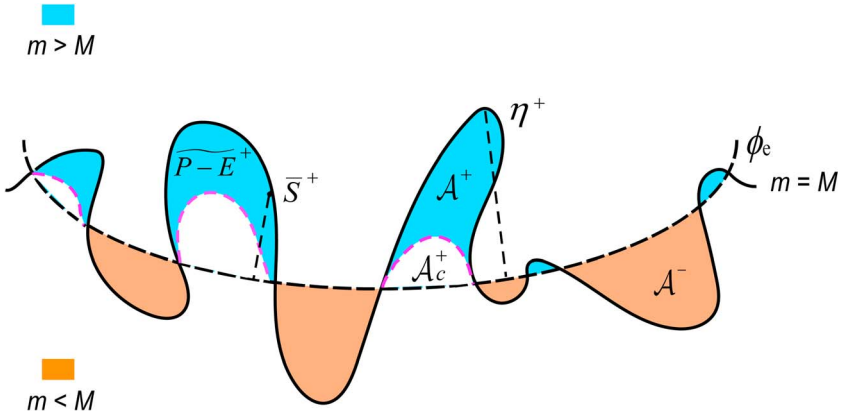

Figure 1. Schematic for the concepts of column integrated water vapor (CWV) local wave activity (LWA) and its sink $\widetilde{P-E}^+$. The solid wavy line denotes an isoline of CWV (M), and the dash line corresponds to the equivalent latitude of M. The northward (southward) intrusion of the M contour is associated with a moist (dry) anomaly, that is, $m > M$ ($m < M$), and the meridional line integral of which gives the local moist wave activity (A^+) and dry wave activity (A^-), respectively. The white areas carved out by the magenta lines correspond to the parts of LWA not participating the hydrological cycle, representing a concept of CWV holding capacity in the face of the meridional disturbances.

budget analysis (illustrated in Figure 1). The main advantage of the areal integration transformation is that the advection of CWV by the rotational component of the moisture flux disappears identically due to the Gauss divergence theorem, thus affording a simpler balance among fewer terms and, more importantly, a tighter linear relationship between CWV wave activity and its sink (denoted as $(\widetilde{P-E})^+$) with their regression slope indicating the HCR. See Lu et al. (2018) and next section for further details about the formulation of the CWV wave activity budget and the associated scaling framework.

Here we extend the CWV activity analysis to summertime regional hydrological cycle, with a focus on the Asian monsoon regions. We first establish the spatial correspondence between the transformed quantity ($(\widetilde{P-E})^+$) and the hydrological extremes represented by the 99.9th percentile of $P - E$, as such inference regarding the former may be translated to the hydrological extremes. The scaling factors associated with the former help to further discern the different characteristics between Indian and East Asian monsoons. Further, it is found that even though the hydrological extremes increase over both Indian and East Asian monsoon regions under future warming, the HCR is strengthened for the former but weakened for the latter. However, the exact dynamical underpinning behind this intriguing result can be complicated and beyond the scope of this study.

2. Data and Methods

2.1. Data

The data sets utilized in the study are the historical (1976–2005) and future (2070–2099) simulations by 16 climate models from the Coupled Model Intercomparison Project Phase 5 (CMIP5; Taylor et al., 2012), the former being forced by the best estimates of the historical forcings and the latter by the Representative Concentration Pathways 8.5 (RCP8.5) forcing scenario, respectively. The number of models chosen is solely based on data availability. To compute the CWV wave activity and the related budget terms, daily outputs of precipitation, evaporation, and specific humidity and wind at all vertical levels are needed. To test the Clausius-Clapeyron scaling, daily 850-hPa air temperature is also used.

2.2. Formulation of Local CWV Finite-Amplitude Wave Activity Budget

As the CWV wave activity is a relatively novel approach to understanding regional hydrological cycle, it is necessary to recapitulate its definition and the associated concept. For any field such as CWV (m) that decreases monotonically with latitude in general, the equivalent latitudes of the field can be defined as

$$\phi_e(M) = \arcsin\left(1 - \frac{\iint_{m\le M} \cos\ \phi d\ \lambda d\ \phi}{2\pi}\right), \tag{1}$$

so that the area enclosed poleward of contour M (upper case for its Lagrangian property) equals that poleward of latitude ϕ_e. Obviously, m in the area resulting from the poleward intrusion of the M contour is always larger than M (see Figure 1). As such, a one-to-one relationship between M and the equivalent latitude ϕ_e is established. With the identification of the equivalent latitude, a pair of line-integral transformations to m (Chen et al., 2015; Huang & Nakamura, 2017; Lu et al., 2018) can be defined for each longitude λ:

$$\mathscr{L}^{-}[m(\lambda,\phi_e)]\equiv\frac{a}{\cos\phi_e}\int_{m\le M,\phi\le\phi_e}m(\lambda,\phi)\cos\phi d\phi, \tag{2a}$$

$$\mathscr{L}^{+}[m(\lambda,\phi_e)]\equiv\frac{a}{\cos\phi_e}\int_{m\ge M,\phi\ge\phi_e}m(\lambda,\phi)\cos\phi d\phi, \tag{2b}$$

where superscript + (−) indicates the meridional interval associated with moist (dry) intrusions, respectively, and the corresponding wave activities will be referred to as moist LWA (A^+) and dry LWA (A^-), as illustrated in Figure 1. Since only the moist extremes are the subject of interest in this study, we will be only focusing on A^+ and the associated budget terms. Analogous to the budget equation of CWV, the major sink/source term of the moist LWA A^+ is $(\widetilde{P-E})^+$, which is the $\mathscr{L}^+$ transformation of $P-E$. As demonstrated in Lu et al. (2018), there exists a tighter linear relationship between A^+ and $(\widetilde{P-E})^+$ even at model grid scale, compared to the relationship between $P-E$ and CWV at a fixed grid (see Figure S1 in the supporting information). Thus, an empirical linear relationship emerges:

$$(\widetilde{P-E})^+\sim\frac{A^+-A_c^+}{\tau}, \tag{3}$$

where τ gives the time scale for the sink $(\widetilde{P-E})^+$ to dissipate the CWV LWA toward the baseline state A_c^+, which is the intercept resulted from the regression of $(\widetilde{P-E})^+$ against A^+ and can be interpreted as the maximum background water vapor intrusions without incurring a phase change or sink, or alternatively, the background water vapor holding capacity in the face of the disturbances (marked symbolically as the magenta line in Figure 1). As such, only the $A^+-A_c^+$ portion participates in the hydrological cycle (blue areas in Figure 1) and is subject to the dissipation by $(\widetilde{P-E})^+$. This leads to the definition of participation ratio (PR) of LWA to the hydrological cycle: $\frac{A^+-A_c^+}{A^+}$. Moreover, τ^{-1} (referred to as HCR) can be interpreted as the rate by which phase change processes work to consume the CWV LWA, a rate reflecting the hydrological cycle in a more local sense. It is worth noting that as $(\widetilde{P-E})^+$ tends to weigh more the extreme values of $P-E$, it represents not only the mean but also the extremes of $P-E$, as to be demonstrated in Figure 2.

By noting that m itself scales with $\frac{\partial M}{\partial y}$ (the Lagrangian meridional gradient of CWV) times the excursion of the air parcel from the corresponding equivalent latitude, we may further scale A^+, a line integral of m, as $-\frac{1}{2}\eta^{+2}\frac{\partial M}{\partial y'}$ with η^+ representing the scale of the poleward stirring or stretching of the M contour (Figure 1). η^+ reflects the dynamic factor and $\frac{\partial M}{\partial y}$ the thermodynamic factor in A^+ (Lu et al., 2018). Making use of the linear relationship (3), we can develop a scaling for the fractional change of the $\mathscr{L}^+$-transformed hydrological cycle:

$$\frac{\delta(\widetilde{P-E})^+}{(\widetilde{P-E})^+}\approx\frac{\delta\left(\frac{A^+-A_c^+}{A^+}\right)}{\left(\frac{A^+-A_c^+}{A^+}\right)}+\frac{\delta A^+}{A^+}+\frac{\delta\tau^{-1}}{\tau^{-1}}\approx\frac{\delta\left(\frac{A^+-A_c^+}{A^+}\right)}{\left(\frac{A^+-A_c^+}{A^+}\right)}+\frac{\delta\left(\frac{\partial M}{\partial y}\right)}{\left(\frac{\partial M}{\partial y}\right)}+\frac{2\delta\eta^+}{\eta^+}+\frac{\delta\tau^{-1}}{\tau^{-1}}. \tag{4}$$

Thus, the fractional change of $(\widetilde{P-E})^+$ can be decomposed into the fractional changes in PR, $\frac{\partial M}{\partial y}$, moisture stirring length scale (η^+), and HCR (τ^{-1}). We will examine each term in equation (4) that contributes to the fractional change of $(\widetilde{P-E})^+$ in the Asian monsoon regions to shed some light on the dynamic and thermodynamic contributions to the changes in the hydrological cycle in these regions.

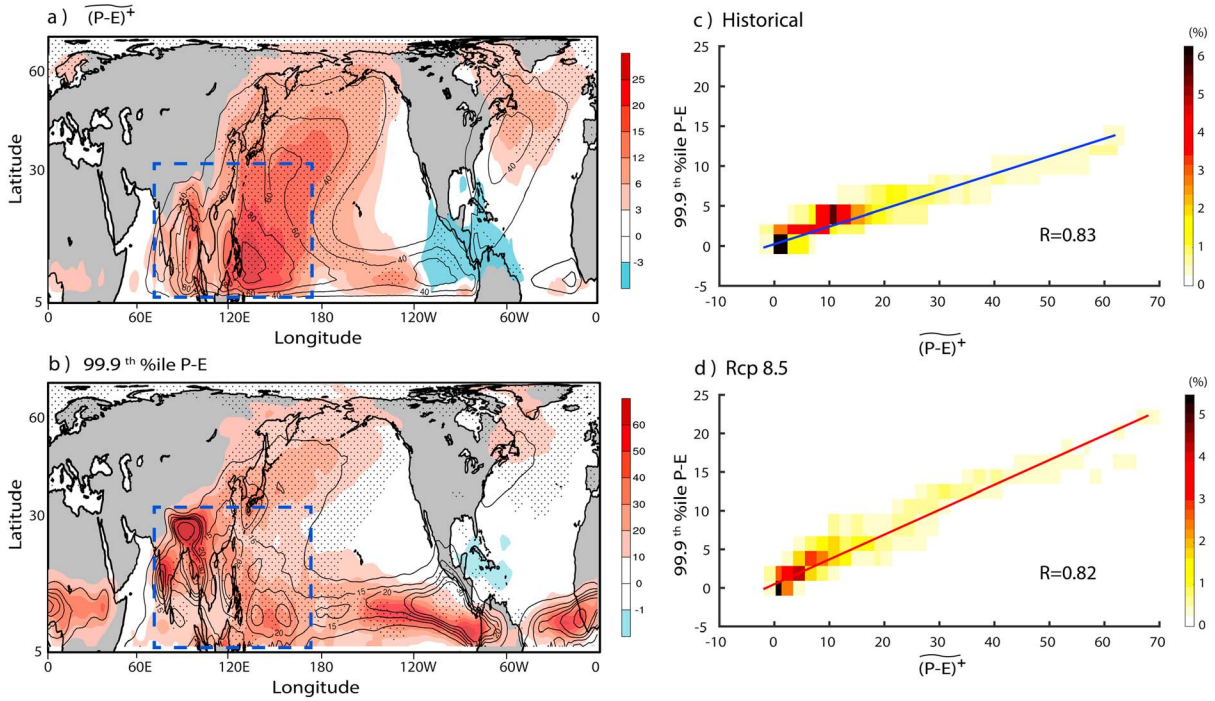

Figure 2. The climatology (contours) and the change (shaded) under the RCP8.5 forcing scenario of (a) $(\widetilde{P-E})^+$ and (b) $(P-E)^{99.9th}$. The black dots denote more than 80% agreement on the sign of the change among 15 CMIP5 models. (c) Two-dimensional probability density distribution of area averaged $(\widetilde{P-E})^+$ and $(P-E)^{99.9th}$ over the Asian monsoon region demarcated by the dashed box in (a) for historical simulations. (d) The same as (c), but for the RCP8.5 simulations. The linear regression slopes are shown in solid lines in (c) and (d).

3. Results

3.1. Correspondence Between the Wave Activity Sink and Extreme Precipitation

Figure 2a shows the multimodel mean historical summertime $(\widetilde{P-E})^+$ (contours) and its change (shading) under RCP8.5 scenario forcing. The high loadings of the historical $(\widetilde{P-E})^+$ pick out the summer storm track regions in the ocean as well as the Asian monsoon regions, such as the Indian subcontinent, Bay of Bengal, and the eastern seaboard of Asia. Under climate warming, $(\widetilde{P-E})^+$ in these regions all increase, reflecting a wet-get-wetter pattern of the response (e.g., Held & Soden, 2006). The corresponding summer mean and change of the 99.9th percentile of $P-E$ (denoted by $(P-E)^{99.9th}$, hereafter) are displayed in Figure 2b, from which one can see immediately their spatial correspondence with the $(\widetilde{P-E})^+$ fields. The features of $(\widetilde{P-E})^+$ are slightly displaced equatorward compared with those of $(P-E)^{99.9th}$, due to the fact that the computed wave activity budget terms are reported at the equivalent latitude (ϕ_e), which is always equatorward of the moist intrusion features as illustrated in Figure 1. The spatial correspondence between the seasonal means of these two quantities at the grid points within the boxed region (70°–170°E, 5°–35°N) in Figure 1a are illustrated by their joint probability density distributions and their regression in Figure 2c, with a correlation coefficient at 0.83 (Figure 2c). Similar spatial correlation is also found between them in the future climate simulations under RCP8.5 forcing scenario (Figure 2d), while the regression slope is somewhat higher than the historical slope, implying that in the future $(\widetilde{P-E})^+$ may represent lower percentile than the 99.9th. Given the spatial relationship between $(\widetilde{P-E})^+$ and $(P-E)^{99.9th}$, inference about the $(\widetilde{P-E})^+$ should have immediate bearing on the hydrological extremes.

3.2. Future Changes of Hydrological Extremes in the Asian Monsoons

Building on the linear relationship between the moist LWA and $(\widetilde{P-E})^+$ (exemplified in Figure S1) and the related scaling (4), we are now able to examine the contributing factors in the local hydrological extremes

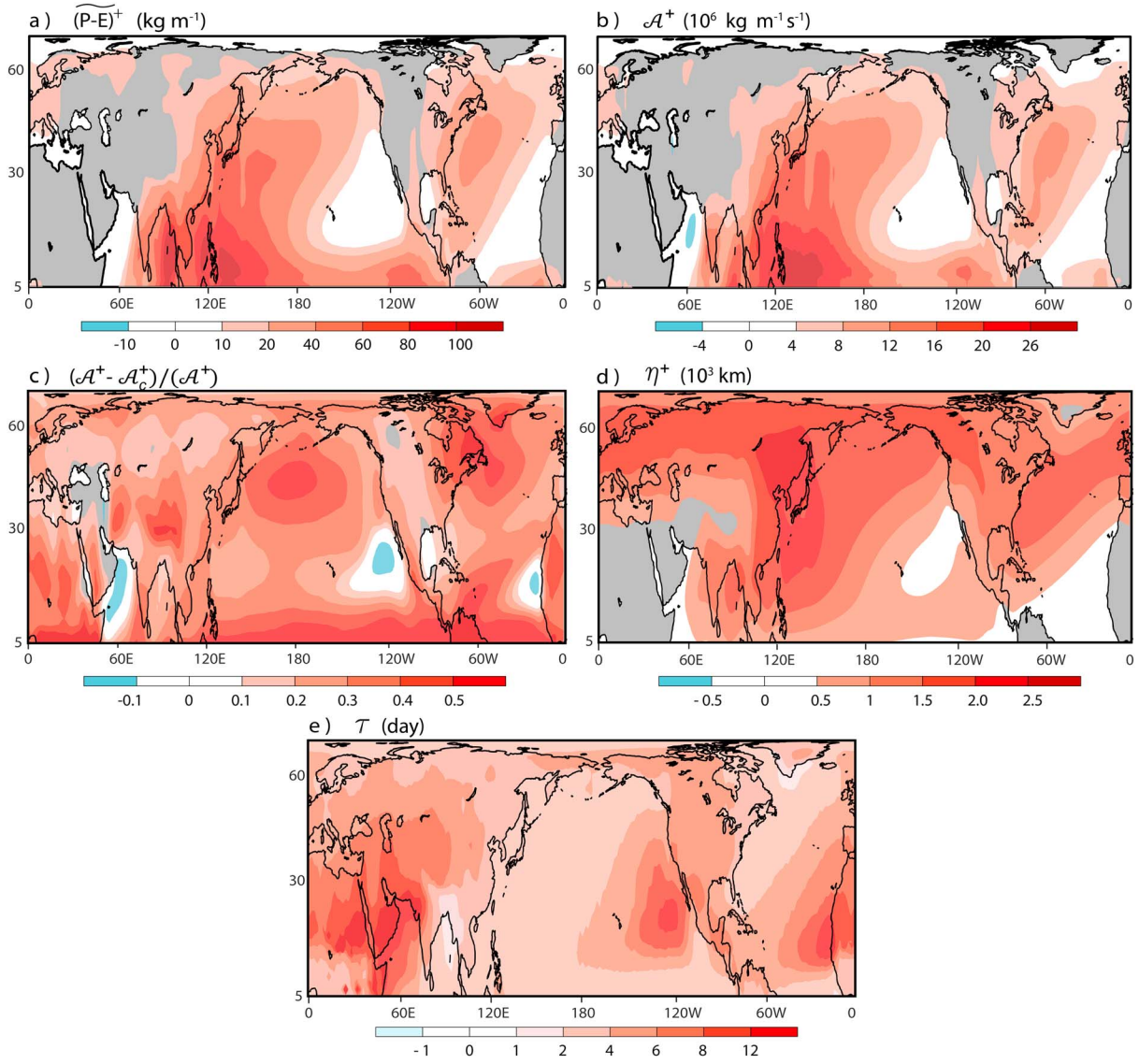

Figure 3. Climatological distribution of summertime (a) $\widetilde{(P-E)}^{+}$, (b) A^{+}, (c) participation ratio $\left(A^{+}-A_c^{+}\right)/(A^{+})$, (d) stirring scale η^{+}, and (e) residence time τ based on the ensemble average of each quantity over 16 CMIP5 models.

$\widetilde{(P-E)}^{+}$: moist wave activities (A^{+}), PR ($\left(A^{+}-A_c^{+}\right)/A^{+}$), stirring scale ($\eta^{+}$), and the resident time (τ). Figure 3 shows the summer climatological feature of each term averaged over 16 CMIP5 models. Apparently, the spatial feature of $\widetilde{(P-E)}^{+}$ strongly resembles that of A^{+} because of their strong linear relationship, with Asian and west Pacific monsoon regions standing out with characteristics of larger A^{+} and $\widetilde{(P-E)}^{+}$ (Figures 3a and 3b). The PR pattern reveals an intriguing distinction between the rainfall in the tropical monsoons and that in the midlatitude storm track (Figure 3c). PR tends to be small in the former, implicative of the larger background water holding capacity associated with warmer temperature and hence less moisture in the poleward intrusions that participates in precipitation. In contrast, PR is much larger (can be >50%) at the core of the storm track in the middle of the north Pacific, implicative of the warmer origin of the air parcels in the poleward intrusions relative to the colder background over the north Pacific, so higher portion of moisture in the midlatitude storms participates in precipitation. An important exception is the high PR over the Himalayas, which can be attributed to the condensation caused by topographic lifting of air parcels. The pattern of the poleward stirring scale η^{+} also reveals a

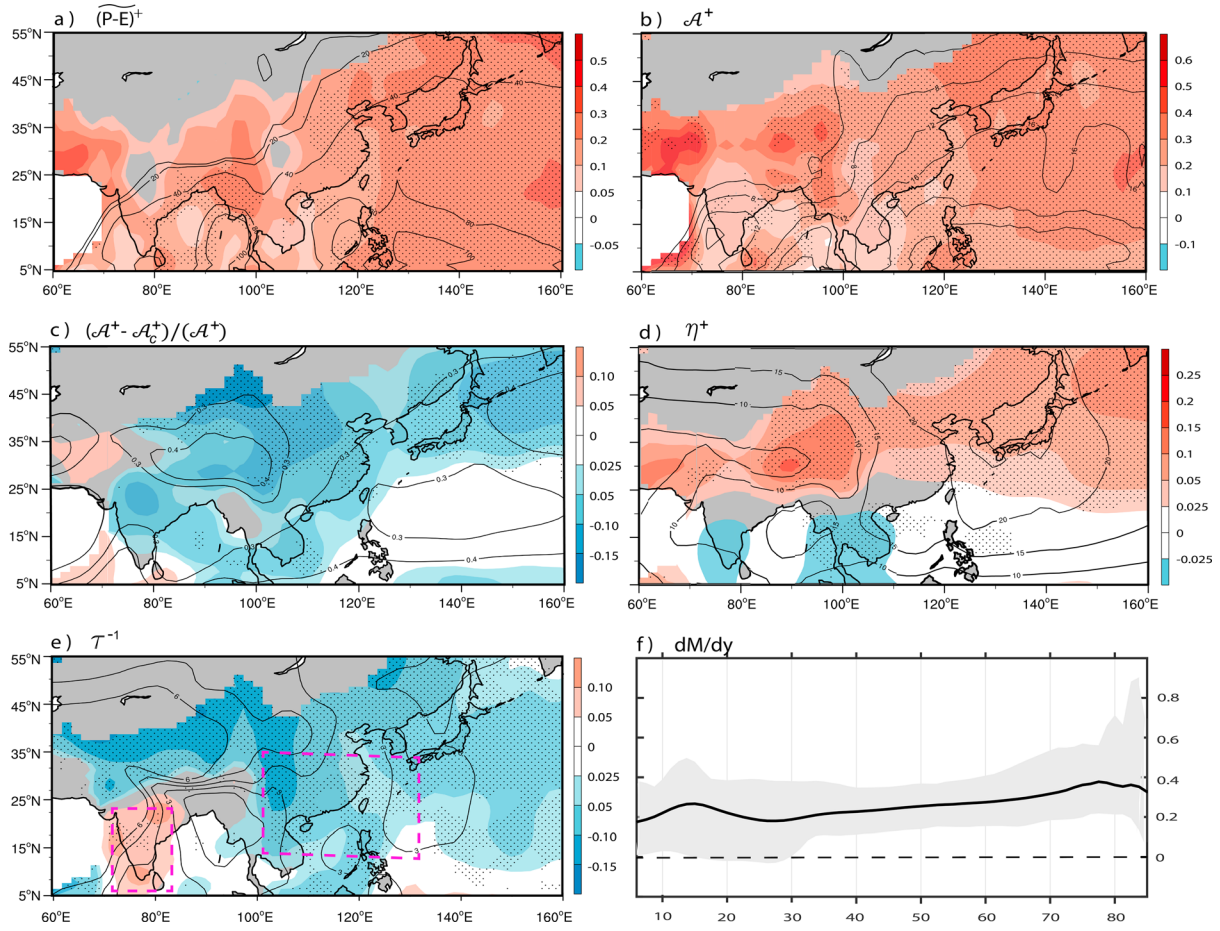

Figure 4. The fractional change of $\widetilde{(P-E)}^{+}$ and those in its scaling factors: (a) $\widetilde{(P-E)}^{+}$, (b) A^{+}, (c) $(A^{+}-A_c^{+})/(A^{+})$, (d) η^{+}, (e) hydrological rate (τ^{-1}), and (f) the Lagrangian gradient of column integrated water vapor (dM/dy) with the range of the intermodel spread expressed in gray shading. In panels (a)–(e), the corresponding background climatology of each is displayed as contours and the dots indicate regions where >80% of the models agreement on the sign of the change.

unique characteristic of the East Asian monsoon: Air parcels travel longer distances poleward before they precipitate compared to the case of the south Asian monsoon (Figure 3d). Meanwhile, large $\widetilde{(P-E)}^{+}$ in both tropical monsoonal regions and the midlatitude storm track means a rather short resident time for the CWV (less than 4 days; Figure 3e). In addition, the same LWA analysis with ERA-I reanalysis data (Figure S2) gives qualitatively similar climatological characteristics of each factor as in Figure 3.

Per equation (4), the fractional change of hydrological extremes measured by $\widetilde{(P-E)}^{+}$ under future warming can be attributed to that of PR, A^{+}, and local HCR. Focusing on Asian monsoon regions (blue box in Figure 4), we find that both moist wave activities A^{+} and $\widetilde{(P-E)}^{+}$ increase over the broad Asian monsoon region under the RCP8.5 warming scenario with a modest intermodel consensus for the South Asian monsoon region and relatively higher consensus for the East Asian monsoon region (Figures 4a and 4b). Intriguingly, the pattern of the ensemble mean increase of $\widetilde{(P-E)}^{+}$ bears considerable resemblance to the most detectable climate change pattern in summer rainfall (Srivastava & DelSole, 2014). The contribution of the thermodynamic component (*dM/dy*) is relatively uniform over a broad range of latitudes (~20%, Figure 4f), while the dynamical factor (η^{+}, Figure 4d) exhibits a meridional dipole in its change, manifesting the poleward shift of the monsoon circulation noticed in CMIP5 projections (e.g., Sandeep & Ajayamohan, 2015). In particular, the negative change of η^{+} over India and Indochina, though weak, is in keeping with the weakening of the horizontal monsoon wind widely documented in literatures (Annamalai et al., 2013; Li et al., 2017; Sandeep et al., 2018; Turner & Annamalai, 2012; Ueda et al., 2006). PR decreases almost everywhere over south and east Asia (Figure 4c), meaning a

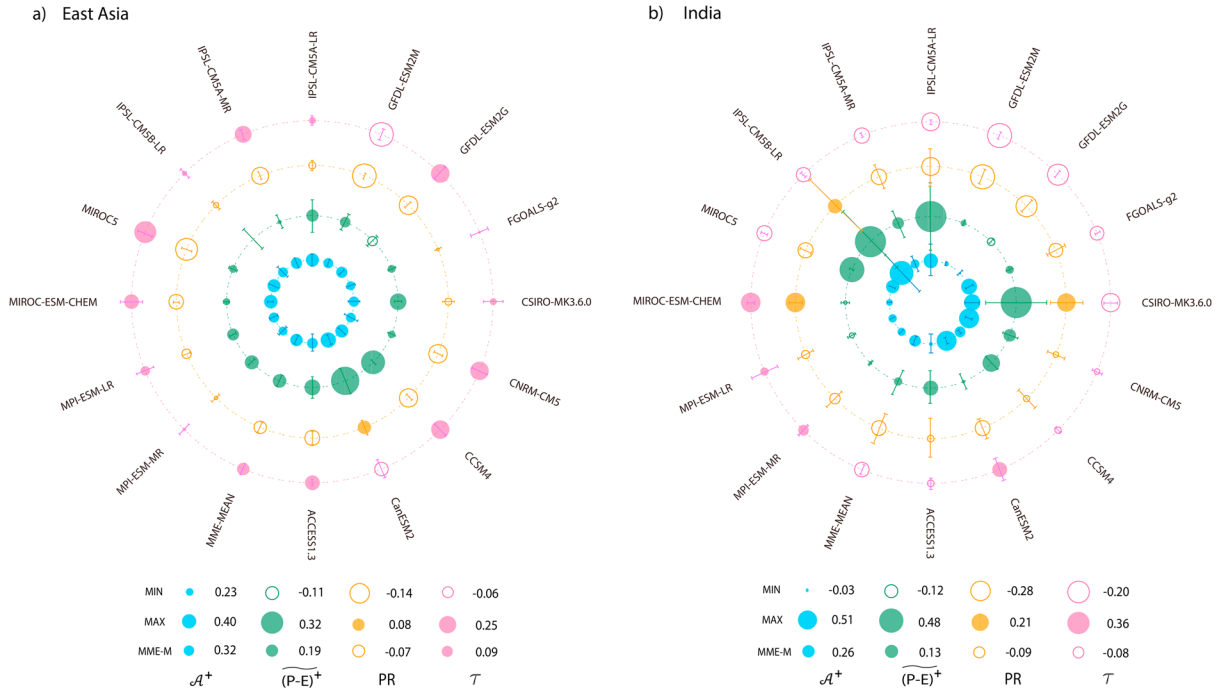

Figure 5. The fractional change of $(\widetilde{P-E})^+$, A^+, $(A^+ - A_c^+)/(A^+)$, and τ averaged over (a) Southeast Asian monsoon and (b) Indian monsoon regions under the RCP8.5 forcing scenario for each of the 16 CMIP5 models. The two domains for the regional average are marked by the magenta boxes in Figure 4e). The filled (open) circle denotes fractional increase (decrease) with the magnitude of the change indicated by the legend. The error bars are the 95% confidence intervals, indicating the uncertainties of the estimated changes in each of the parameters for each model. The same scale as the diameter of the circle is applied to the length of the error bars, so that the fractional change is statistically insignificant if the error bar is longer than the diameter of the circle, or not confined within the circle.

greater proportion of the moisture not participating in the hydrological cycle in the summer monsoon systems as climate warms. This is likely the result of larger temperature increases over land and the oceans nearby to its east (e.g., Kirtman et al., 2013) relative to the temperature increase over the regions of the water vapor source (Mei et al., 2015). On the other hand, HCR exhibits intriguing contrasting behavior between Indian monsoon (left magenta box in Figure 4e) and other Asian monsoon regions, with an intensification for the former (~10%) and a weakening for the latter (~−12%). This means it will take longer time to dissipate the moist wave activity in the warmer future climate over East Asian monsoon region but less time over Indian monsoon region, even though $(\widetilde{P-E})^+$ increases about the same (~20%) over these two regions. The underlying mechanisms for the increase in $(\widetilde{P-E})^+$ in the two regions might differ given their distinct change in HCR, a topic warranting further investigation.

To gain more confidence in the characteristics discussed above, we further check A^+, $(\widetilde{P-E})^+$, PR, and HCR averaged over Southeast Asian monsoon region (Figure 5a) and Indian monsoon region (Figure 5b), respectively, in each of the 16 CMIP5 models. Under the forcing of RCP8.5 scenario, all models simulate an increased moist wave activity over Southeast Asian monsoon region and 13 out the 16 models capture an increase in $(\widetilde{P-E})^+$. Meanwhile, PR decreases in all except one model. The response of the HCR is slightly less robust; still, 80% of the models project a decrease in HCR over the Southeast Asia. For Indian monsoon region, the responses in A^+, $(\widetilde{P-E})^+$, PR, and HCR exhibit similar robustness, except that the sign of the HCR response is opposite: 13 out of 16 models project an intensification of HCR (Figure 5b). The modest robustness across the models examined thus lends us some confidence in the projected intensification of the hydrological extremes in Asian monsoons under climate warming. Note that the modest agreement across models should not be interpreted as the statistical significance of the changes. We have examined the uncertainties in all the four parameters (see the supporting information) and found that the changes are only significant in a limited number of models (Figure 5).

4. Conclusion and Discussion

Column integrated water vapor LWA is utilized in this study to examine the projected changes of hydrological cycle in the future global warming scenario of the CMIP5 models. The geometrically transformed $P - E$ is found to be spatially correlated with the precipitation extremes especially over Asian monsoon regions, so any insight gained on the response of the former may be translated into that on the latter. Further, the tight temporal linear relationship between $(\widetilde{P-E})^+$ and moist LWA offers a different perspective for interpreting the hydrological cycle in the monsoon regions: Monsoon rainfall can be thought of as the result of air parcels being disturbed meridionally from their source regions (this is especially true for the East Asian monsoon) with the moisture they carry condensing efficiently as quantified by the small moisture residence time.

Under the RCP 8.5 warming scenario, both Indian monsoon and the east and southeast Asian monsoon regions will undergo a relatively robust intensification in the hydrological cycle measured by $(\widetilde{P-E})^+$. Although it is not entirely new that both the mean and the extremes of precipitation over the Asian monsoon region will intensify under greenhouse gas forcing (e.g., Sooraj et al., 2015; Turner & Annamalai, 2012; Turner & Slingo, 2009; Pfahl et al., 2017), the current investigation based on the line-integral transformation of the hydrological quantities results in somewhat better consensus, even on the change of the circulation factor. In particular, the scaling of $(\widetilde{P-E})^+$ reveals an increased rate of the local HCR over Indian subcontinent, in stark contrast to the other Asian monsoon regions and the hydrological cycle in winter season. As the enhanced HCR is related to a steeper characteristic slope of the air parcel trajectory feeding into the monsoon system (see Scaling for HCR in the supporting information), the HCR increase here seems to be in broad agreement with the upward vertical velocity anomalies over India subcontinent seen in CMIP projections, despite a general weakening of tropical circulation elsewhere (e.g., Vecchi & Soden, 2007) and a weakening of the Indian monsoon circulation as depicted by the weakening of the meridional tropospheric temperature gradient and vertical wind shear (Mei et al. 2015). The modest consensus on the geometrically transformed hydrological quantities may be attributed to the fact that they weigh the extreme values more than the non-extremes through the geometric transformation; therefore, they are more representative of the hydrological extremes than the median values. For Asian monsoons, indeed, CMIP models seem to converge robustly on the warming-induced increase in the extreme categories of monsoonal rainfall (Kitoh et al., 2013; Lau et al., 2017; Pfahl et al., 2017; Sooraj et al., 2015).

Last, we must admit that although the wave activity based scaling can help shed some fresh light on the thermodynamic and circulation factors in the hydrological cycle of the monsoon systems, the approach is fundamentally diagnostic. Asian monsoons are among the most complicated subsystems of our climate system, involving complex interplay among factors like the shape and properties of land, topography, elevated heating, convection, moisture sources, and the nonlinear fluid dynamics of the ocean and atmosphere. It remains a grand challenge to understand and predict how monsoon would behave under different external climate forcings.

Acknowledgments
We like to thank the two anonymous reviewers for their valuable comments that helped improve the presentation of the manuscript significantly. We are also grateful to Jesse Norris for confirming the positive circulation contribution to the high precipitation percentiles over Indian monsoon region in CESM large ensemble simulations. This work is supported by the U.S. Department of Energy Office of Science Biological and Environmental Research (BER) as part of the Regional and Global Climate Modeling Program. The Pacific Northwest National Laboratory is operated for the Department of Energy by Battelle Memorial Institute under contract DE-AC05-76RL01830. D. X. is supported by the National Natural Science Foundation of China (Grants 41475092, 41621005, and 41775073). Y. Z. is supported by the National Natural Science Foundation of China (Grants 41475092 and 41621005). X. D. is jointly supported by China Scholarship Council (CSC) and Jiangsu Collaborative Innovation Center for Climate Change. The authors also acknowledge the World Climate Research Programme's Working Group on Coupled Modeling, which is responsible for CMIP, and we thank the climate modeling groups for producing and making available their model output. CMIP5 data can be accessed via https://esgf-node.llnl.gov/search/cmip5/.

References

Allen, M. R., & Ingram, W. J. (2002). Constraints on future changes in the hydrological cycle. *Nature*, *419*(6903), 224–232. https://doi.org/10.1038/nature01092

Annamalai, H., Hafner, J., Sooraj, K. P., & Pillai, P. (2013). Global warming shifts the monsoon circulation, drying South Asia. *Journal of Climate*, *26*, 2701–2718.

Chen, G., Lu, J., Burrows, D. A., & Leung, L. R. (2015). Local finite-amplitude wave activity as an objective diagnostic of midlatitude extreme weather. *Geophysical Research Letters*, *42*, 10,952–10,960. https://doi.org/10.1002/2015GL066959

Held, I. M., & Soden, B. J. (2006). Robust responses of the hydrological cycle to global warming. *Journal of Climate*, *19*(21), 5686–5699. https://doi.org/10.1175/JCLI3990.1

Huang, C. S. Y., & Nakamura, N. (2017). Local finite-amplitude wave activity as a diagnostic of anomalous weather events. *Journal of the Atmospheric Sciences*, *73*(1), 211–229. https://doi.org/10.1175/JAS-D-15-0194.1

Kirtman, B., Power, B. S., Adedoyin, A. J., Boer G. J., Bojariu, R., & Camilloni, I., et al. (2013). Near-term climate change: Projections and predictability. In climate change 2013: The physical science basis, working group I contribution to the IPCC 5th assessment.

Kitoh, A., Endo, H., Krishna Kumar, K., Cavalcanti, I. F. A., Goswami, P., & Zhou, T. (2013). Monsoons in a changing world: A regional perspective in a global context. *Journal of Geophysical Research: Atmospheres*, *118*, 3053–3065. https://doi.org/10.1002/jgrd.50258

Lau, K. M., Kim, K. M., & Leung, L. Y. (2017). Competing influences of greenhouse warming and aerosols on Asian summer monsoon circulation and rainfall. *Asia-Pacific Journal of Atmospheric Sciences*, *53*(2), 181–194. https://doi.org/10.1007/s13143-017-0033-4

Li, G., Xie, S. P., He, C., & Chen, Z. (2017). Western pacific emergent constraint lowers projected increase in Indian summer monsoon rainfall. *Nature Climate Change*, *7*(10), 708–712. https://doi.org/10.1038/nclimate3387

Lu, J., Sakaguchi, K., Yang, Q., Leung, L. Y., Chen, G., Zhao, C., et al. (2017). Examining the hydrological variations in an aquaplanet world using wave activity transformation. *Journal of Climate*, *30*(7), 2559–2576. https://doi.org/10.1175/JCLI-D-16-0561.1

Lu, J., Xue, D., Gao, Y., Chen, G., Leung, L. Y., & Staten, P. W. (2018). Enhanced hydrological extremes in the western United States under global warming through the lens of water vapor wave activity. *Climate and Atmospheric Science*, *1*(1). https://doi.org/10.1038/s41612-018-0017-9

Meehl, G. A., Stocker, T. F., Collins, W. D., Friedlingstein, P., Gaye, A. T., Gregory, J. M., et al. (2007). *Chapter 10: Global climate projections, working group I contribution to the fourth assessment report of Intergovernmental Panel on Climate Change*. UK and New York, USA: Cambridge University Press.

Mei, R., Ashfaq, M., Rastogi, D., Leung, L. R., & Dominquez, F. (2015). Dominating controls for wetter South Asian monsoon in the twenty-first century. *Journal of Climate*, *28*, 3400–3419.

Neiman, P. J., Schick, L. J., Ralph, F. M., Hughes, M., & Wick, G. A. (2011). Flooding in western Washington: The connection to atmospheric rivers. *Journal of Hydrometeorology*, *12*(6), 1337–1358. https://doi.org/10.1175/2011JHM1358.1

Pall, P., Allen, M. R., & Stone, D. A. (2007). Testing the Clausius-Clapeyron constraint on changes in extreme precipitation under co warming. *Climate Dynamics*, *28*(4), 351–363. https://doi.org/10.1007/s00382-006-0180-2

Pendergrass, A. G., & Hartmann, D. L. (2014). The atmospheric energy constraint on global-mean precipitation change. *Journal of Climate*, *27*(2), 757–768. https://doi.org/10.1175/JCLI-D-13-00163.1

Pfahl, S., O'Gorman, P. A., & Fischer, E. M. (2017). Understanding the regional pattern of projected future changes in extreme precipitation. *Nature Climate Change*, *7*(6), 423–427. https://doi.org/10.1038/nclimate3287

Ralph, F. M., Neiman, P. J., Wick, G. A., Gutman, S. I., Dettinger, M. D., Cayan, D. R., et al. (2006). Flooding on California's Russian river: The role of atmospheric rivers. *Geophysical Research Letters*, *33*, L13801. https://doi.org/10.1029/2006GL026689

Sandeep, S., & Ajayamohan, R. S. (2015). Poleward shift in Indian summer monsoon low level jet stream under global warming. *Climate Dynamics*, *45*(1-2), 337–351. https://doi.org/10.1007/s00382-014-2261-y

Sandeep, S., Ajayamohan, R. S., Boos, W. R., Sabin, T. P., & Praveen, V. (2018). Decline and poleward shift in Indian summer monsoon synoptic activity in a warming climate. *Proceedings of the National Academy of Sciences of the United States of America*, *115*(11), 2681–2686. https://doi.org/10.1073/pnas.1709031115

Santer, B. D., Mears, C., Wentz, F. J., Taylor, K. E., Gleckler, P. J., Wigley, T. M. L., et al. (2007). Identification of human-induced changes in atmospheric moisture content. *Proceedings of the National Academy of Sciences of the United States of America*, *104*(39), 15,248–15,253. https://doi.org/10.1073/pnas.0702872104

Sooraj, K. P., Terray, P., & Mujumdar, M. (2015). Global warming and the weakening of the Asian summer monsoon circulation: Assessments from the CMIP5 models. *Climate Dynamics*, *45*(1-2), 233–252. https://doi.org/10.1007/s00382-014-2257-7

Srivastava, A. K., & DelSole, T. (2014). Robust forced response in South Asian summer monsoon in a future climate. *Journal of Climate*, *27*(20), 7849–7860. https://doi.org/10.1175/JCLI-D-13-00599.1

Stephens, G. L., & Hu, Y. X. (2010). Are climate-related changes to the character of global-mean precipitation predictable? *Environmental Research Letters*, *5*(2), 025209. https://doi.org/10.1088/1748-9326/5/2/025209

Taylor, K. E., Stouffer, R. J., & Meehl, G. A. (2012). An overview of CMIP5 and the experiment design. *Bulletin of the American Meteorological Society*, *93*(4), 485–498. https://doi.org/10.1175/BAMS-D-11-00094.1

Trenberth, K. E., Dai, A., Rasmussen, R. M., & Parsons, D. B. (2003). The changing character of precipitation. *Bulletin of the American Meteorological Society*, *84*(9), 1205–1218. https://doi.org/10.1175/BAMS-84-9-1205

Turner, A. G., & Annamalai, H. (2012). Climate change and the South Asian summer monsoon. *Nature Climate Change*, *2*(8), 587–595. https://doi.org/10.1038/nclimate1495

Turner, A. G., & Slingo, J. M. (2009). Subseasonal extremes of precipitation and active-break cycles of the Indian summer monsoon in a climate-change scenario. *Quarterly Journal of the Royal Meteorological Society*, *135*(640), 549–567. https://doi.org/10.1002/qj.401

Ueda, H., Iwai, A., Kuwako, K., & Hori, M. E. (2006). Impact of anthropogenic forcing on the Asian summer monsoon as simulated by eight GCMs. *Geophysical Research Letters*, *33*, L06703. https://doi.org/10.1029/2005GL025336

Vecchi, G. A., & Soden, B. J. (2007). Global warming and the weakening of the tropical circulation. *Journal of Climate*, *20*(17), 1529–1530.

Zhu, Y., & Newell, R. E. (1998). A proposed algorithm for moisture fluxes from atmospheric rivers. *Monthly Weather Review*, *126*(3), 725–735. https://doi.org/10.1175/1520-0493(1998)126<0725:APAFMF>2.0.CO;2